Available online at www.sciencedirect.com

ScienceDirect

journal homepage: www.intl.elsevierhealth.com/journals/dema

Effects of ZnO/TiO_2 nanoparticle and TiO_2 nanotube additions to dense polycrystalline hydroxyapatite bioceramic from bovine bones

Luara Aline Pires[a], *Lucas José de Azevedo Silva*[b], *Brunna Mota Ferrairo*[b], *Rogério Erbereli*[c], *João Fiore Parreira Lovo*[c], *Orisson Ponce Gomes*[d], *José Henrique Rubo*[b], *Paulo Noronha Lisboa-Filho*[d], *Jason Alan Griggs*[e], *Carlos Alberto Fortulan*[c], *Ana Flávia Sanches Borges*[a,*]

[a] *Department of Operative Dentistry, Endodontics and Dental Materials, Bauru School of Dentistry, University of São Paulo, Alameda Dr. Octávio Pinheiro Brisolla, 9-75, Vila Universitária, 17012-901 Bauru, SP, Brazil*

[b] *Department of Prosthodontics and Periodontics, Bauru School of Dentistry, University of São Paulo, Alameda Dr. Octávio Pinheiro Brisolla, 9-75, Vila Universitária, 17012-901 Bauru, SP, Brazil*

[c] *Department of Mechanical Engineering, São Carlos School of Engineering, University of São Paulo, Avenida Trabalhador São-Carlense, 400, Centro, 13566-590 São Carlos, SP, Brazil*

[d] *Department of Physics, School of Sciences, São Paulo State University, Av. Engenheiro Luiz Edmundo Carrijo Coube, s/n, Vargem Limpa, 17033360 Bauru, SP, Brazil*

[e] *Department of Biomedical Materials Science, School of Dentistry, University of Mississippi Medical Center, 2500 North State Street, Room D528, 39216-4505 Jackson, MS, United States*

ARTICLE INFO

Keywords:
Ceramics
Durapatite
Nanoparticles
Nanotubes

ABSTRACT

Objectives. A bovine dense hydroxyapatite ceramic (HA) was produced as new biomaterial, however, the production of a material with consistently high flexural strength remains challenging. The objective of this study was to evaluate the effects of ZnO nanoparticles, TiO_2 nanoparticles, and TiO_2 nanotubes (1%, 2%, and 5% by weight) on the microstructure and flexural strength of a bovine dense hydroxyapatite ceramic (HA).

Methods. Discs (Ø = 12.5 mm; thickness = 1.3 mm) were prepared and subjected to X-ray diffraction (XRD), and observation with a field emission scanning electron microscope (FE-SEM), biaxial flexural strength (BFS) testing, and Vickers hardness (VH) testing. The BFS and VH data were subjected to ANOVA and Tukey post-hoc tests ($\alpha = 0.05$) and Weibull analysis.

Results. The XRD showed that the addition of nanomaterials caused the formation of a secondary phase when 5% of the ZnO nanoparticles was used, or when all percentages of the TiO_2 nanoparticles/nanotubes were used, and the HA crystallographic planes were maintained. Differences were not observed between the higher BFS values obtained with pure HA

* *Corresponding author.*
E-mail addresses: luara.pires86@hotmail.com (L.A. Pires), lucasjazevedos@usp.br (L.J. de Azevedo Silva), brunna.ferrairo@usp.br (B.M. Ferrairo), rogerio.erbereli@usp.br (R. Erbereli), joao.lovo@ifsp.edu.br (J.F.P. Lovo), orisson.gomes@unesp.br (O. Ponce Gomes), jrubo@usp.br (J.H. Rubo), paulo.lisboa@unesp.br (P.N. Lisboa-Filho), jgriggs@umc.edu (J.A. Griggs), fortulan@usp.br (C.A. Fortulan), afborges@fob.usp.br (A.F.S. Borges).

https://doi.org/10.1016/j.dental.2019.11.006

and those obtained with the 5% addition of TiO_2 nanoparticles. However, the results were different compared with the other groups ($\alpha = 0.05$). The results obtained by Weibull analysis revealed that the 1%, 2%, and 5% addition of TiO_2 nanotubes, and the 1% and 2% addition of TiO_2 nanoparticles decreased the HA characteristic strength (σ_0), while the Weibull modulus (m) increased when 5% of TiO_2 nanoparticles, 1% and 2% of ZnO nanoparticles, and 2% of TiO_2 nanoparticles were added, but with no statistical difference from the pure HA. The 5% addition of ZnO_2 nanoparticles decreased the σ_0 without changing m. Moreover, the 5% addition of TiO_2 nanoparticles resulted in an m closest to that of pure HA. Regarding the VH results, the blend of HA with 1% and 2% addition of TiO_2 nanoparticles exhibited the higher values, which were similar between the different addition ratios ($p = 0.102$). Moreover, the addition of 5% TiO_2 nanoparticles resulted in higher value compared with pure HA.

Significance. This study demonstrated that the HA blend with 5% of TiO_2 nanoparticles has the greatest potential as a bovine HA dense bioceramic reinforcement.

Significance statement

"A new dense polycrystalline bovine hydroxyapatite bioceramic can be a potentially sustainable material by solid waste recycling, with the addition 5% TiO_2 nanoparticles".

1. Introduction

Meat production has great socioeconomic importance worldwide but raises environmental concerns with regard to the impact caused by the generation of waste, which can be harmful to human health and the environment [1–3]. Bovine bones, such as those obtained from waste, are widely available. Conversely, because of their availability in large quantities at low cost, their reuse can significantly contribute to the reduction of negative environmental impact [2–4].

These bones are sources of hydroxyapatite (HA) $(Ca)_{10}(PO_4)_6(OH)_2$ and in previous studies, the incorporation of HA nanoparticles on the surface of titanium implants resulted in the improvement of their biological characteristics [13–15]. The proposed HA-based implant manufacturing method creates favorable biological conditions [13–16]. Moreover, although it exhibits excellent biocompatibility, bioactivity, and osteoconductivity [5–7,10–12,16,17]. HA has poor mechanical properties, which restrict its clinical applications to artificial teeth and artificial bone [8,11,12]. With regard to the best reuse of bovine HA, the production of dense polycrystalline bovine HA bioceramics may be promising in terms of the produced material combining the chemical advantages of HA and the ability to produce as little solid waste from bovine bones as possible [18–20].

An improvement in the mechanical properties and fracture toughness can be obtained by adding reinforcements in the ceramic matrix [8,21–24]. The improvement in the fracture toughness by the addition of whiskers and nanoparticles in the matrix is based mainly on the processes of crack bridging, crack deflection, and sliding of crack bridging [22,23]. In these processes, the crack propagation energy is absorbed or diverted, and the stress concentration at the crack tip is eliminated or reduced [8,9,21]. Then, an additional increase of the reinforcement is possible, when an array contains particles that may influence the propagation direction of a crack [9,22]. For this purpose, many reinforcing structures have been used to fabricate an HA matrix composition, such as zirconia, titanium, glass, alumina, silver, and carbon, which may form fiber, nanoparticle, or nanotube structures [43,44]. Moreover, this study aimed to produce, and structurally and mechanically characterize, a dense bovine HA bioceramic with 1%, 2%, or 5% addition of TiO_2 nanotubes, TiO_2 nanoparticles, or ZnO nanoparticles. The null hypothesis is that, with the addition of nanostructures, there will be no difference in terms of microstructure, mean and variation of flexural strength, and microhardness.

2. Material and methods

2.1. *Preparation of TiO_2 nanotubes and TiO_2/ZnO nanoparticles*

The TiO_2 nanotubes were obtained by alkaline synthesis according to Arruda et al. [45]. Moreover, 10 g of commercial TiO_2 anatase powder (Aldrich, 99%) were mixed in 120 ml of NaOH (10 M) alkaline solution. The mixture was maintained at 120 °C for 24 h in a Teflon vessel, which was subjected to heating through a glycerin bath, using a heating blanket as the heat source. After 24 h, the NaOH alkaline solution with TiO_2 powder was washed with deionized water and a hydrochloric acid solution (HCl) (0.1 M) sequentially and repeatedly. The samples were washed until finally reaching pH 4. Then, they were dried at 200 °C for 24 h under an air atmosphere, to eliminate the liquid part and obtain the final material (Arruda et al., 2015).

The TiO_2 nanoparticles were obtained using the sol–gel process. Briefly, 185 ml of distilled water, 56.7 ml of isopropanol, and 2.6 ml of nitric acid (HNO_3) were added to an Erlenmeyer flask. Subsequently, 15 ml of titanium(IV) isopropoxide were added to the stirred solution (300 rpm) for 30 min. The solution was heated at 85 °C while stirring. These heating and stirring patterns were maintained until the liquid

had completely evaporated, which resulted in crystallization. Subsequently, the powder resulted after evaporation was taken to the furnace to reduce the homogeneous powder.

The ZnO nanoparticles were obtained using the sol-gel process, and the amorphous ZnO powder was weighed using a digital scale. Deionized water (100 ml) and nitric acid (15 ml) were added to a beaker on a 300 rpm magnet agitator at a temperature of approximately 90 °C, and ZnO was gradually added to the liquid. Then, citric acid (5.50 g) was weighed using a digital scale and gradually added to 190 ml of deionized water contained in another beaker. The two liquid contents were mixed in the larger beaker to react with the citric acid. After waiting for 15 min, ethylene glycol (10.5 ml) was added while stirring for a few hours to initiate the pH measurement at a temperature of approximately 290 °C. After reaching a pH in between 3 and 4, the temperature was reduced to 180 °C while stirring. After crystallization, the beaker was placed in a furnace to reduce the homogeneous powder.

2.2. Preparation of HA powder

Bovine (24 months old) metatarsus samples, which were certified to be free of contamination, were subjected to thermochemical processes to remove organic matter. Additionally, the samples did not include heavy metals in their composition, as required for the production of hydroxyapatite granules (HA).

For the characterization of HA, X-ray diffraction (XRD) was carried out. The best temperature calcination of the bovine bone powders was 900 °C.

2.3. Ceramic disc preparation

The experimental groups were: pure HA; HA/TiO_2npX% (X = 1%, 2%, or 5% of TiO_2 nanoparticles); HA/ZnOnpX% (X = 1%, 2%, or 5% of ZnO nanoparticles); HA/TiO_2ntX% (X = 1%, 2%, or 5% of TiO_2 nanotubes).

The materials used in disc manufacturing were polyvinyl butyral (PVB) (Butvar B98) as the binder, 4-aminobenzoic acid (PABA) as the deflocculant, and isopropyl alcohol as the solvent of the binder and liquid barbotine medium. The ball mill jar was charged with a slurry at a concentration of 30 vol% solids (HA + nanostructures) and 70 vol% vehicle (0.05% PABA and 69.95% isopropyl alcohol). Then, it was rotated at 104 rpm for 48 h and placed in a vibratory mill for another 96 h until reaching 0.35 μm. Subsequently, 1.2 wt% of PVB was added based on the weight of HA, which was mixed and homogenized in a vibratory mill for 2 h.

The nanostructures were added to produce the groups (Table 1), and were again placed in the vibratory mill for an additional 10 min. Subsequently, the jar was discharged, and the barbotine was dried with a hot air blower at approximately 80 °C. This mixture was granulated in sieves with a #200 mesh ≤75 μm to obtain granules with an average size of 35 μm. Then, the granules were pressed into a cylindrical mold according with ISO 6872 [42] with a uniaxial pressure of 100 MPa for 30 s, and they were isostatically pressed in elastomeric balloons for 30 s at a pressure of approximately 206 MPa (30,000 psi). Finally, the HA green discs were sintered in a chamber furnace (Lindberg Blue/M) at a maximum temperature of 1300 °C.

2.4. X-ray diffraction (XRD)

The specimens were positioned in the sample holder to ensure a smooth surface, and they were mounted onto a fixed horizontal sample plane. The spectra were recorded at room temperature using a Philips X' Pert X-ray diffractometer with a Cu Kα source (λ = 1.5418 Å) and Bragg-Brentano geometry (2θ) from 10° to 80°. Data analyses were carried out using the profile fits of selected individual XRD peaks.

2.5. Field emission scanning electron microscopy (FE-SEM)

The surface was observed using a field emission scanning electron microscope (FE-SEM) (JSM-IT300, JEOL, Tokyo, Japan). Before observing the surface, the specimens were polished using silicon carbide papers with grit sizes of #150, #240, #320, #400, #600, #800, and #1200 for 5 min per granulation. Then, the specimens were polished with felt discs and diamond abrasive paste of 4 μm, 2 μm, and 1 μm in a semiautomatic sander (EXACT, Norderstedt, Schleswig-Holstein, Germany). This methodology has been previously described by Magalhaes et al. [28].

2.6. Biaxial flexural strength (BFS)

The specimens were tested by BFS (n = 30) and Weibull analysis according to the ISO 6872 standard (2015). The disk specimens were positioned on three steel balls with a diameter of 3.2 mm and positioned 120° apart on a circle with a diameter of 10 mm, in a universal testing machine (MTS, Eden Prairie, USA). The specimens were loaded by a piston with a diameter of 1.4 mm at a crosshead speed of 0.2 mm/min until fracture. The fracture loads were recorded, and the biaxial flexural strength (σ) was calculated in MPa using the following equation: $\sigma = -0.23870\,P(X-Y)/b^2$, where σ is the maximum tensile stress (MPa), P is the total fracture load (N), and X and Y are calculated as follows: $X = (1+\nu)\ln(r_2/r_3)^2 + [(1-\nu)/2](r_2/r_3)^2$, and $Y = (1+\nu)\ln(r_1/r_3)^2 + [(1-\nu)/2](r_1/r_3)^2$, where ν is Poisson's ratio = 0.25, r_1 is the support circle radius (mm), r_2 is the loaded area radius (mm), r_3 is the specimen radius (mm), and b is the specimen thickness at the fracture origin (mm).

2.7. Vickers hardness (VH)

Five specimens from each group were fixed into PVC cylinders by pouring epoxy resin (Piraglass Ltda., Piracicaba, SP, Brazil) into the cylinders. After polymerization, the surface of each specimen was flattened by silicon carbide papers (#150, #240, #320, #400, #600, #800, and #1200) and polished with felt discs and diamond pastes of 4 μm, 2 μm, and 1 μm in a polisher device (APL-4, Arotec, São Paulo, SP, Brazil) followed by 10 min of sonication (Maxi Clean 750-UNIQUE UltraSonic, Indaiatuba, SP, Brazil).

Table 1 – Density and ratio of components used in specimen preparation.

Component	Density (g/cm^3)	Ratio (%)	Function
HA	3.14	30% (total volume)	Ceramic powder
PABA (4-aminobenzoic acid)	1.37	0.05% (ZrO_2 weight)	Deflocculant
PVB (polyvinyl butyral)	1.1	2% (ZrO_2 weight)	Binder
Isopropyl alcohol	0.78	70% (total volume)	Solvent
TiO2 nanoparticles	4.23	1%, 2%, or 5% (total volume)	Reinforcement
ZnO nanoparticles	5.61		
TiO2 nanotubes	4.23		

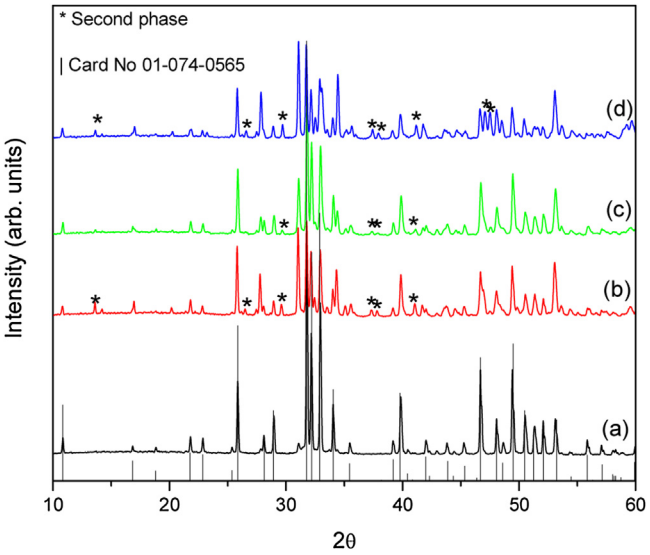

Fig. 1 – XRD patterns of (a) pure, (b) 1%, (c) 2%, and (d) 5% TiO_2 nanoparticles incorporated into HA. Card No 01-074-0565 ($Ca_{10}(PO_4)_6(OH)_2$).

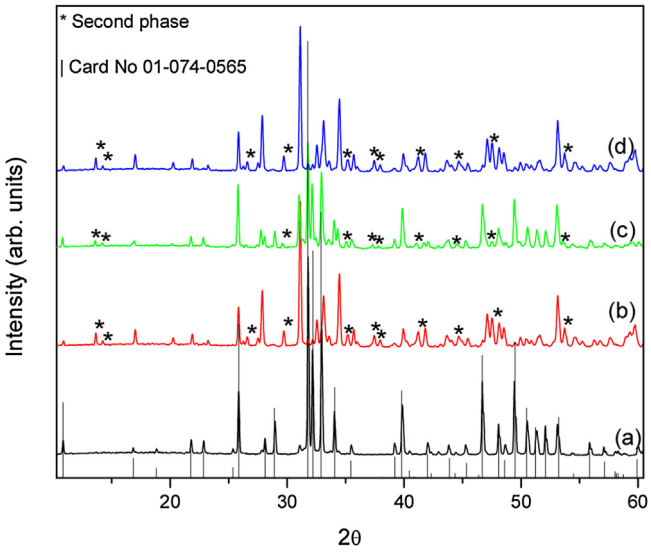

Fig. 2 – XRD patterns of (a) pure, (b) 1%, (c) 2%, and (d) 5% TiO_2 nanotubes incorporated into HA. Card No 01-074-0565 ($Ca_{10}(PO_4)_6(OH)_2$).

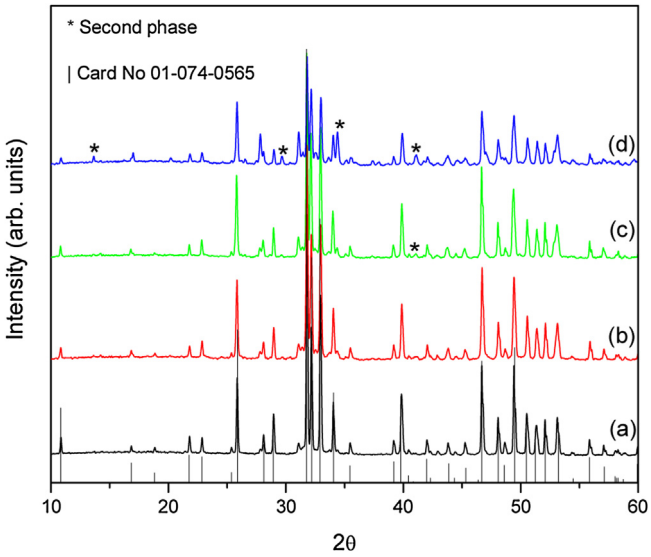

Fig. 3 – XRD patterns of (a) pure, (b) 1%, (c) 2%, and (d) 5% ZnO nanoparticles incorporated into HA. Card No 01-074-0565 ($Ca_{10}(PO_4)_6(OH)_2$).

The VMHT MOT hardness machine (Leica, Wetzlar, Germany) containing a Vickers diamond was used. A load of 200 gf was applied for 15 s. Five indentations were recorded on the surface of each specimen. The distance between each indentation was 100 mm. The mean hardness number was calculated for each specimen and group, and these values were recorded.

2.8. *Statistical analysis*

The BFS and hardness data were assessed using one-way analysis of variance (ANOVA), followed by multiple comparisons amongst the groups using the Tukey post-hoc test at $\alpha = 0.05$.

Weibull analysis (Weibull 7++, Reliasoft, Tucson, USA) using maximum likelihood estimation was also performed for the BFS data. The Weibull modulus (m) and characteristic strength (σ_0) were obtained for each group (with 95% confidence intervals).

3. Results

3.1. *XRD results*

The XRD results for the samples are presented in Figs. 1–3. The spectra are shown according to the three addition percentages of the TiO_2 nanotubes and TiO_2/ZnO nanoparticles in the HA. The XRD spectra exhibited a certain crystallographic disorder, owing to the addition of nanomaterials. However,

Table 2 – BFS data in MPa (different letters indicate statistical significance of 5% ($p < 0.05$)).

Groups	Mean ± standard deviation
HA	235,2 ± 36,5 a
HA/TiO_2nt 1%	129,4 ± 33,4 b
HA/TiO_2nt 2%	119,9 ± 25,1 b
HA/TiO_2Nt 5%	120,8 ± 8,0 b
HA/TiO_2np 1%	140,2 ± 26,8 b
HA/TiO_2np 2%	88,0 ± 9,1 c
HA/TiO_2np 5%	214,9 ± 36,4 a
HA/ZnOnp 1%	125,2 ± 24,0 b
HA/ZnOnp 2%	141,9 ± 22,5 b
HA/ZnOnp 5%	86,4 ± 12,5 c

Table 3 – VH Data in GPa (different letters indicate statistical significance of 5% ($p < 0.05$)).

Groups	Mean ± standard deviation
HA/TiO_2np 1%	455.4 ± 22.32 a
HA/TiO_2np 2%	432.5 ± 18.22 a
HA/ZnOnp 5%	400.9 ± 15.17 b
HA/TiO_2np 5%	399.6 ± 15.31 b
HA/ZnOnp 2%	376.3 ± 13.27 b
HA	335 ± 12.98 c
HA/TiO_2nt 1%	317.4 ± 16.67 c
HA/TiO_2nt 2%	310.2 ± 9.85 c,d
HA/TiO_2nt 5%	286.9 ± 28.72 d
HA/ZnOnp 1%	260.5 ± 11.34 e

the predominance of the crystallographic planes of HA was maintained (card#01-074-0565). Additionally, it was possible to identify the formation of a secondary phase, regardless of the type of nanomaterials (Figs. 1–3). In the case of ZnO, the formation was more accentuated for the 5% sample. In the samples with 1% and 2% addition of ZnO nanoparticles, the secondary phase was not identified. However, in the case of the TiO_2 nanoparticles/nanotubes, even with a 1% addition of nanostructures, the calcium phosphate ($Ca_3(PO_4)_2$ and titanium phosphate secondary phases could be observed.

3.2. *FE-SEM results*

The FE-SEM images (2500× magnification) in Fig. 4B show the HA/TiO_2nt1% with various larger grains and more merging occurring amongst them (white arrows), and the presence of pores (Fig. 4B), compared with pure HA (Fig. 4A). The HA/ZnOnp1% (Fig. 4C) exhibits larger grains compared with pure HA, and volumetric defects (arrows). The HA/TiO_2np1% (Fig. 4D) exhibits a mix of grains similar to pure HA and larger grains (white arrows). When 2% of nanomaterials is used (HA/TiO_2nt2%; Fig. 4E) the observed pattern of larger grains was the same as that observed in HA/TiO_2nt1% (Fig. 4B). The HA/ZnOnp2% (Fig. 4F) exhibited characteristics similar to those of HA/ZnOnp1% (Fig. 4C) and lesser pores while the HA/TiO_2np2% (Fig. 4G) exhibited larger grains and few pores. The HA/ZnOnp5% (Fig. 4H) exhibited a higher prevalence of larger grains compared with pure HA. The HA/TiO_2nt5% (Fig. 4I) also produced larger grains with various agglomerate sites and pores. With a nanomaterial addition of 5%, the HA/TiO_2np5% (Fig. 4J) exhibited smaller grains, which were nevertheless larger than those of pure HA. Additionally, many agglomerate-like sites (arrows) were also observed.

3.3. *BFS results*

The HA and HA/TiO_2np5% exhibited higher values without any differences. However, these values were different to those of other groups ($p = 0.067$). The HA/ZnOnp5% and HA/TiO_2np2% exhibited lower values without any differences ($p = 1$). The other groups exhibited intermediate results (Table 2).

3.4. *Weibull analysis results*

The Weibull analysis results revealed that the HA/TiO_2np1%, HA/ZnOnp1%, and HA/TiO_2nt1% decreased the σ_0 and resulted in a statistically similar m value, compared with pure HA, without any differences being observed (Fig. 5A). The HA/ TiO_2np2% exhibited higher σ_0 than HA/ZnOnp2% and HA/TiO_2nt2% without any differences in m values, but these values were lower than those obtained for pure HA (Fig. 5B). The HA/TiO_2np5% obtained the best results of experimental groups for σ_0 and m were statistically equal to those obtained for pure HA. A higher m value was obtained for HA/TiO_2nt5%, but its σ_0 was between the better results and the results obtained for HA/ZnOnp5%, which exhibited the lowest σ_0 values (Fig. 5C).

3.5. *VH results*

Regarding the VH results, the blend of HA with 1% and 2% addition of TiO_2 nanoparticles exhibited the higher values, which were similar between them ($p = 0.102$). Moreover, the addition of 5% TiO_2 nanoparticles resulted in higher value compared with pure HA. The HA/ZnOnp2%, HA/ZnOnp5%, and HA/TiO_2np5% exhibited the second higher values without no difference between them; however, these values were lower compared with those of the HA/TiO_2np1% and HA/TiO_2np2%. The HA, HA/TiO_2nt1%, and HA/TiO_2nt2% exhibited intermediate values without any differences ($p = 0.054$). The HA/ZnOnp1% exhibited lower values, which were different to those obtained for the groups exhibiting higher and intermediate values ($p = 0.05$). The HA/TiO_2nt5% exhibited similar values without any differences to the values obtained for HA/TiO_2nt2% ($p = 0.089$) (Table 3).

4. Discussion

The choice of using nanostructures to enhance the mechanical properties is justified by the crack deflection mechanism reported by Faber and Evans [22]. This mechanism is based on the increase of fracture toughness, owing to the crack deflection caused by the nanoparticles. The crack profile of materials with nanoparticle additions exhibited a deflection pattern, which approximately corresponds to the nanoparticle grain size, while the materials without nanoparticle additions exhibited fairly smooth crack patterns compared with the other materials [23]. However, it is important to note that with a higher ceramic firing temperature, the possibility of densification and agglomeration for the nanoparticles became greater [22]. Note that the agglomeration and densification processes can influence the microstructure by decreasing

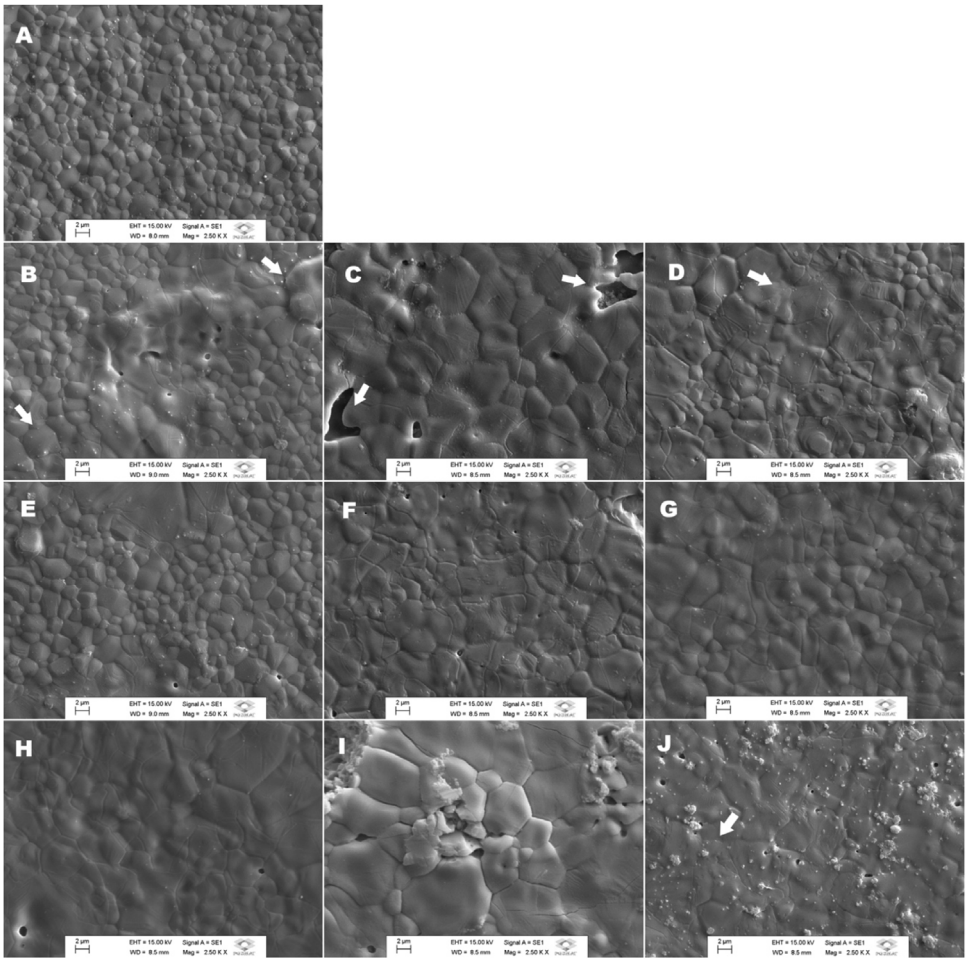

Fig. 4 – FE-SEM of groups in same sequence of graphs shown in Fig. 4. A. Pure HA (control). B, C, D. Groups with 1% TiO_2 nanotubes (HA/TiO_2nt1%), 1% ZnO nanoparticles (HA/ZnOnp1%), and 1%vTiO_2 nanoparticles (HA/TiO_2np1%), respectively. E, F, G. Groups with 2% of TiO_2 nanotubes (HA/TiO_2nt2%), 2% TiO_2 nanoparticles (HA/TiO_2np2%), and 2% ZnO nanoparticles (HA/ZnOnp2%), respectively. H, I, J. Groups with 5% ZnO nanoparticles (HA/ZnOnp5%), 5% TiO_2 nanotubes (HA/TiO_2nt5%), and 5% TiO_2 nanoparticles (HA/TiO_2np5%), respectively.

the mechanical strength and generating localized internal stresses, which result in critical micro cracking [24].

The XRD patterns observed in this study did not exhibit nanoparticle or nanotube phases that are particular to a composite material, regardless of TiO_2 or ZnO additions. The anatase, brookite, and rutile, which are the three polymorphic phases of TiO_2 observed under ambient conditions [25], were not detected. The spectral patterns indicate phases' mixture between the HA components and the nanoparticles/nanotubes, which resulted in the formation of a secondary phase and a new material characterized as a solid solution. Some solid solutions can be weaker than others. The FE/SEM images show that this mixture could have increased the grain size and caused the creation of some pores (arrows) (Fig. 4B, F, G, and I). A previous study conducted by Miranda et al. [35] discussed the reduction of density in the Y-TZP/TiO_2 composite through the addition of TiO_2. These and previous results [36] indicate the incorporation of TiO_2 as a reason for formatting the pores in the material. However, it is possible to reduce the amount of porosity within the material by optimizing the sintering time and temperatures [35,36]. Thus, the higher the grain size is, the lower is the cohesive strength [35,37,38].

The flexural strength results were subjected to Weibull analysis. The Weibull contour plots were used to determine the difference between the groups. The non-overlapping contour plots indicate differences amongst the investigated groups. The reliability was calculated for each group to evaluate the potential use of restorative frameworks. According to the Weibull analysis, higher values were observed for σ_0 and m in HA/TiO_2np5%. Moreover, these are the best results of BFS, and they did not have any differences compared with the results obtained for pure HA, although they were different from the results obtained for the other groups. Previous results obtained by Magalhães et al. [28] have revealed that the incorporation of TiO_2 nanotubes in Y-TZP can influence the material's structure. Additionally, it has been shown that the increase of the m values leads to the improved reliability of the experimental Y-TZP, despite the decrease of its flexural strength [34]. A higher *m* value indicates higher

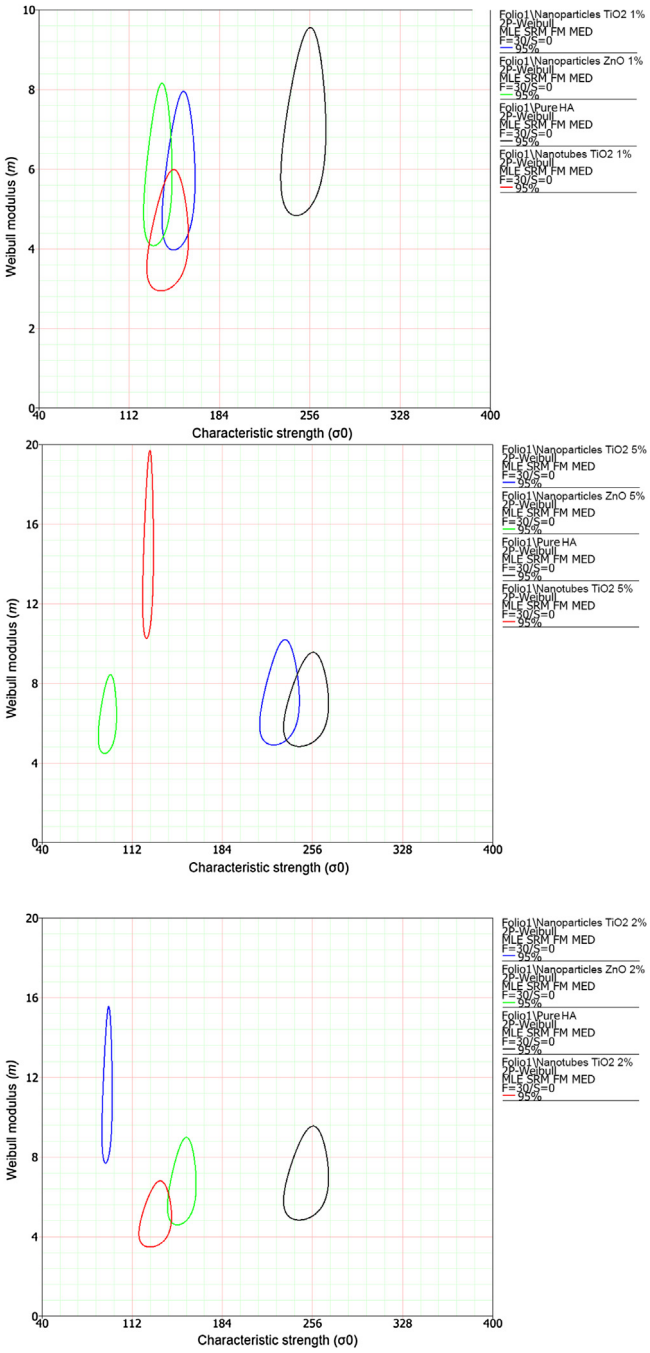

Fig. 5 – Weibull plot for groups compared with that of pure HA, and fracture stress as function of fracture probability. A. Groups with 1% TiO_2 nanotubes (HA/TiO_2nt1%), 1% ZnO nanoparticles (HA/ZnOnp1%), and 1% TiO_2 nanoparticles (HA/TiO2np1%). B. Groups with 2% TiO_2 nanotubes (HA/TiO_2nt2%), 2% TiO_2 nanoparticles (HA/TiO_2np2%), and 2% ZnO nanoparticles (HA/ZnOnp2%). C. Groups with 5% ZnO nanoparticles (HA/ZnOnp5%), 5% TiO_2 nanotubes (HA/TiO_2nt5%), and 5% TiO_2 nanoparticles (HA/TiO_2np5%).

predictability in the mechanical behavior of ceramic materials [39]. In this study, this was assumed to indicate that the TiO_2 nanoparticles had one of the best reinforcement nanostructures compared with other tested nanostructures, which is in agreement with the results obtained by previous studies [21,26–29]. One study [30] investigated the addition of TiO_2 nanoparticles in epoxy nanocomposites, and despite the different nature of the tested material, it was found that the maximum improvement of nanoparticles was at approximately 10 wt%, which increased the flexural strength. However, a decrease of up to 20 wt% of the nanoparticle content, owing to particle clustering, was also observed. With regard to the mechanical strength of the brittle materials investigated in this study, the results obtained for the biaxial flexural strength were least variable. Using a circular specimen on three spaced points, the maximum tensile stress was produced at the center of the specimen surface, where the fracture typically originates [21].

According to Anusavice et al. [40], hardness is defined as the resistance of a material to plastic deformation, which is a surface property typically produced by an indentation force and acts as a first protection against mechanical challenges to the materials. In this study, it was observed that the group with the added TIO_2 nanoparticles had the higher values. Specifically, the addition of 1% and 2% of TiO_2 nanoparticles resulted in higher values compared with the other groups.

A previous study conducted by Goyat et al. [31] revealed that the TiO_2 nanotubes added in HA could possibly increase the microhardness. These results were similar to the results obtained by other studies wherein TiO_2 nanoparticles were incorporated in HA [32,33]. However, the demonstrated applications of these studies were different to those considered in this study. According to Rempel et al. [41], the grain size decreases with the increase of microhardness. These results are similar to those obtained in this study with the 5% addition of TiO_2 nanoparticles, which resulted in bigger grain sizes compared with the other addition amounts (1% and 2%), decreasing their VH values. Additionally, the results were similar to the results obtained for pure HA (Fig. 4J and A). However, the 5% addition of TiO_2 nanoparticles resulted in higher values compared with the values obtained for pure HA. The best matching results were obtained by connecting the study results (XRD, FE-SEM, and BFS), becoming it more reliable compared to the others.

The results obtained in this study predict that increasing the weight percent of TiO_2 nanoparticles may provide an approach toward further investigating the mechanical properties of HA-based ceramics. Thus, it is important to study the BFS, fracture toughness, and biocompatibility in future work.

5. Conclusions

Considering the limitations of this study, it was concluded that the incorporation of 5% TiO_2 nanoparticles showed the best combinations of microstructure, flexural strength, reliability maintenance, and superior hardness.

Acknowledgments

The authors are grateful for the financial support provided by the São Paulo Research Foundation (FAPESP; process numbers: 2018/23639-0 and 2013/07296-2; CDMF/CEPID/FAPESP) and the National Council for Scientific and Technological Development (CNPq; process number: 154705/2015-2).

REFERENCES

[1] Yukalang N, Clarke B, Ross K. Solid waste management solutions for a rapidly urbanizing area in Thailand: recommendations based on stakeholder input. Int J Environ Res Public Health 2018;15(July (7)):1302.

[2] Arvanitoyannis IS, Ladas D. Meat waste treatment methods and potential uses. Int J Food Sci Technol 2008;43(March (3)):543–59.

[3] Jayathilakan K, Sultana K, Radhakrishna K, Bawa A. Utilization of byproducts and waste materials from meat, poultry and fishprocessing industries: a review. J Food Sci Technol 2012;49(3):278–93.

[4] Berkun M, Aras E, Anilan T. Solid waste management practices in Turkey. J Mater Cycles Waste Manag 2011;13(December (4)):305–13.

[5] Bagambisa FB, Joos U, Schilli W. Mechanisms and structure of the bond between bone and hydroxyapatite ceramics. J Biomed Mater Res 1993;27:1047–56.

[6] Eanes ED. The influence of fluoride on the seeded growth of apatite from stable supersaturated solutions at pH 7.4. J Dent Res 1980;59(February (2)):144–50.

[7] Liu C, Wang W, Shen W, Chen T, Hu L, Chen Z. Evaluation of the biocompatibility of a nonceramic hydroxyapatite. J Endod 1997;23(8):490–3.

[8] Fang Z, Feng Q, Tan R. In-situ grown hydroxyapatite whiskers reinforced porous HA bioceramic. Ceram Int 2013;39:8847–52.

[9] Fortulan CA. Compósito alumina-zircônia: obtença˜o através de conformaça˜o coloidal e caracterizaça˜o microestrutural. Sa˜o Carlos: Relatório de Pós-doutorado-Universidade Federal de Sa˜o Carlos; 1999. p. 82.

[10] Dutta SR, et al. Ceramic and non-ceramic hydroxyapatite as a bone graft material: a brief review. Iran J Med Sci 2015;184(1):101–6.

[11] Jäger M, Jennissen H, Dittrich F, Fischer A, Köhling H. Antimicrobial and osseointegration properties of nanostructured titanium orthopaedic implants. Materials 2017;10(11):1302.

[12] Gamelas JAF, Martins AG. Surface properties of carbonated and non-carbonated hydroxyapatites obtained after bone calcination at different temperatures. Colloids Surf A Physicochem Eng Asp 2015;478(August):62–70.

[13] Kweon H, Lee SW, Hahn BD, Lee YC, Kim SG. Hydroxyapatite and silk combination coated dental implants result in superior bone formation in the peri implant area compared with hidroxyapatite and collagem combination-coated implants. J Oral Maxillofac Surg 2014;72(October (10)):1928–36.

[14] Hung K, Lo SC, Shih CS, Yang YC, Feng HP, Lin YC. Titanium surface modified by hydroxyapatite coating for dental implants. Surf Coat Technol 2013;231(September):337–45.

[15] Roy M, Bandyopadhyay A, Bose S. Induction plasma sprayed nano hydroxyapatite coatings on titanium for orthopaedic and dental implants. Surf Coat Technol 2011;205(8):2785–92.

[16] Rau JV, Cacciotti I, De Bonis A, Fosca M, Komlev VS, Latini A, et al. Fe-doped hydroxyapatite coatings for orthopedic and dental implant applications. Appl Surf Sci 2014;307(July):301–5.

[17] Dorozhkin SV. Bioceramics of calcium orthophosphate. Biomaterials 2010;31(7):1465–85.

[18] Hench LL. Bioceramics: from concept to clinic. J Am Ceram Soc 1991;74:1487–510.

[19] Cao W, Hench LL. Bioactive materials. Ceram Int 1996;22:493–507.

[20] Hench LL. Bioceramics. J Am Ceram Soc 1998;81:1705–28.

[21] Rezaee M, Khoie SMM, Liu KH. The role of brookite in mechanical activation of anatase- to-rutile transformation of nanocrystalline TiO_2: An XRD and Raman spectroscopy investigation. CrystEngComm 2011;13(16):5055–61.

[22] Faber KT, Evans AG. Crack deflection processes-I. Theory. Acta Metallurgica 1983;31(4):565–76.

[23] Fathi H, Miller C, Stokes C, Johnson A. The effect of ZrO_2 and TiO_2 on solubility and strength of apatite-mullite glass-ceramics for dental applications. J Mater Sci Mater Med 2014;25(3):583–94.

[24] Yoshida K, Nishiyama N, Shinoda Y, Akatsu T, Wakai F. Evaluation of effects of crack deflection and grain bridging on toughening of nanocrystalline SiO_2 stishovite. J Eur Ceram Soc 2017;37(15):5113–7.

[25] Heimann RB. Materials science of crystalline bioceramics: a review of basic properties and applications. CMU J 2002;1:23–46.

[26] Kalita SJ, Somani V. Al_2TiO_5–Al_2O_3–TiO_2 nanocomposite: structure, mechanical property and bioactivity studies. Mater Res Bull 2010;45(12):1803–10.

[27] Stanciu L, Groza JR, Stoica L, Plapcianu C. Influence of powder precursors on reaction sintering of Al_2TiO_5. Scr Mater 2004;50(May (9)):1259–62.

[28] Magalhães APR, Fortulan CA, Lisboa-Filho PN, Ramos-Tonello CM, Gomes OP, Cesar PF, et al. Effects of Y-TZP blank manufacturing control and addition of TiO_2 nanotubes on structural reliability of dental materials. Ceram Int 2018;44(February (3)):2959–67.

[29] Kalita SJ, Qiu S, Verma S. A quantitative study of the calcination and sintering of nanocrystalline titanium dioxide and its flexural strength properties. Mater Chem Phys 2008;109(2):392–8.

[30] Fathi HM, Johnson A. The effect of TiO_2 concentration on properties of apatite-mullite glass-ceramics for dental use. Dent Mater 2016;32(February (2)):311–22.

[31] Goyat MS, Rana S, Halder S, Ghosh PK. Facile fabrication of epoxy-TiO_2 nanocomposites A critical analysis of TiO_2. Ultrason Sonochem 2018;40(January):861–73.

[32] Shirdar MR, Taheri MM, Sudin I, Shafaghat A, Keyvanfar A, Majid MZ. In situ synthesis of hydroxyapatite grafted titanium nanotube composite. J Exp Nanosci 2016;11(July (10)):816–22.

[33] Oktar FN. Hydroxyapatite TiO_2 composites. Mater Lett 2006;60:2207–10.

[34] Que W, Khor KA, Xu JL, Yu LG. Hydroxyapatite/titânia nanocomposites derived by combining high-energy ball milling with spark plasma sintering processes. J Eur Ceram Soc 2008;28:3083–90.

[35] Miranda RBP, Miranda WG, Lazar DRR, Ussui V, Marchi J, Cesar PF. Effect of titania content and biomimetic coating on the mechanical properties of the Y-TZP/TiO_2 composite. Dent Mater 2018;34(February (2)):238–45.

[36] Miao X, Sun D, Hoo PW, Liu J, Hu Y, Chen Y. Effect of titania addition on yttria-stabilised tetragonal zirconia ceramics sintered at high temperatures. Ceram Int 2004;30(6):1041–7.

[37] Eichler J, Rödel J, Eisele U, Hoffman M. Effect of grain size on mechanical properties of submicrometer 3Y-TZP: fracutre strength and hydrothermal degradation. J Am Ceram Soc 2007;90(September (9)):2830–6.

[38] Stawarczyk B, Özcan M, Hallmann L, Ender A, Mehl A, Hämmerlet C. The effect of zirconia sintering temperature on flexural strength, grain size and contrast ratio. Clin Oral Investig 2013;17(1):269–74.

[39] Yoshimura HN, Molisani AL, Narita NE, Cesar PF, Goldenstein H. Porosity dependence of elastic constants in aluminum nitride ceramics. Mater Res 2007;10(June (2)):127–33.
[40] Anusavice KJ, Shen C, Rawls HR. Philips' science of dental materials. 12th ed. Saunders: Elsevier; 2012.
[41] Rempel SV, Bogdanova EA, Valeeva AA, Schroettner H, Sabirzyanov NA, Rempel AA. Microhardness and phase composition of TiO y/hydroxyapatite nanocomposites synthesized under low-temperature annealing conditions. Inorg Mater 2016;52(May (5)):476–82.
[42] International Standard ISO 6872. Dentistry—ceramic materials. Geneva, Switzerland: International Standards Organization; 2015.
[43] Zapata PA, Rabagliati FM, Lieberwirth I, Catalina F, Corrales T. Study of the photodegradation of nanocomposites containing TiO2 nanoparticlesdispersed in polyethylene and in polyethylene-co-octadecene. Polym Degrad Stab 2014;109:106–14.
[44] Costa ACFM, Vilar MA, Lira HL, Kiminami RHGA, Gama L. Síntese e caracterização de nanopartículas de TiO2. Cerâmica 2006;52(324):255–9.
[45] Arruda LB, Santos CM, Orlandi MO, Schreiner WH, Lisboa PN. Formation and evolution of TiO2 nanotubes in alkaline synthesis. Ceram Int 2015;41(2):2884–91.